Carbohydrate Polymers 87 (2012) 2593–2604

Contents lists available at SciVerse ScienceDirect

Carbohydrate Polymers

journal homepage: www.elsevier.com/locate/carbpol

Controlling the thickness of polymeric shell on magnetic nanoparticles loaded with doxorubicin for targeted delivery and MRI contrast agent

Sumanta Kumar Sahu[a], Swatilekha Maiti[b], Arindam Pramanik[a], Sudip Kumar Ghosh[b], Panchanan Pramanik[a,*]

[a] Department of Chemistry, Indian Institute of Technology, Kharagpur 721 302, West Bengal, India
[b] Department of Biotechnology, Indian Institute of Technology, Kharagpur 721 302, West Bengal, India

ARTICLE INFO

Article history:
Received 18 March 2011
Received in revised form 14 June 2011
Accepted 11 November 2011
Available online 22 November 2011

Keywords:
Magnetic nanoparticles
Chitosan
Doxorubicin
Targeted drug delivery
Cancer therapy

ABSTRACT

The polymeric functionalization of superparamagnetic iron oxides nanoparticles is developed for cancer targeting capability and magnetic resonance imaging. Here the nanoparticles (NP) are decorated through the adsorption of a polymeric layer around the particle surface for the formation of core–shell. The synthesized magnetic nanoparticles (MNPs) are conjugated with fluorescent dye, targeting ligand, and drug molecules for improvement of target specific diagnostic and possible therapeutics applications. In this investigation doxorubicin was loaded into the shell of the MNPs and release study was carried out at different pH. The core–shell structure of magnetic NP coated chitosan matrix was visualized by TEM observation. The cytotoxicity of these magnetic NPs is investigated using MTT assay and receptor mediated internalization by HeLa and NIH3T3 cells are studied by fluorescence microscopy. Moreover, compared with T_2-weighted magnetic resonance imaging (MRI) in the above cells, the synthesized nanoparticles are showed stronger contrast enhancements towards cancer cells.

1. Introduction

Amongst the broad spectrum of nanoscale materials being investigated for biomedical use, the MNPs have created significant interest due to their intrinsic magnetic properties for guided delivery of drugs and contrast agents for magnetic resonance imaging (MRI) (Dilnawaz, Singh, Mohanty, & Sahoo, 2010; Park et al., 2008; Thierry, Winnik, Merhi, Silver, & Tabrizian, 2003; Thierry et al., 2005). In order to fully exploit the potential of MNPs for image guided drug delivery upon systemic administration, they should be biocompatible, stable in the circulation, and the potential for prolonged circulation in the blood stream. This can be circumvented by coating the MNPs with hydrophilic polymers that preferably give them 'stealth' properties. The coatings with hydrophilic polymers were carried out to improve their colloidal stability and also prolong circulation kinetics (Basti et al., 2010; Hafeli et al., 2009; Kim, Kim, Kim, & Lee, 2009; Wan et al., 2007). However, the above coated MNPs have limited drug loading capacity and the rapidly dissociation after administration for drug delivery purposes. Polyethylene glycol and dextran are the most widely used polymers for drug delivery purposes (Kohler, Fryxell, & Zhang, 2004; Lin et al., 2009; Zhang, Srivastava, & Misra, 2007). The stability and targeting efficiency of NPs are the two most important factors for the successful application to drug delivery and diagnostic imaging. Special coating of the materials is required to provide both stability and multi-functionality to MNPs. MNPs were coated with a shell of stable and biocompatible material to avoid its potential toxic effects on the cells (Dobson, 2006; Fang & Zhang, 2009; McCarthy, Kelly, Sun, & Weissleder, 2007). The targeting ligands are specially needed to immobilize onto NP surfaces for targeted drug delivery. The materials currently available for NPs coating are generally compromised with required levels of stability and multi-functionality. Recently, the development of a facile, economical, and simple strategy for synthesis of monodisperseable hydrophilic size controlled superparamagnetic NPs without using any surfactants is a highly challenging matter of research. In this article, a simple and low cost (all the reagents employed are economical) process was designed to synthesize monodispersed superparamagnetic NPs for targeted anticancer drug delivery. The carboxymethyl chitosan (CMC) is an amphoteric polyelectrolyte that derived from chitosan is already extensively used in a wide range of biomedical applications (Liang et al., 2008; Liu, Chen, Lin, & Liu, 2006; Prabaharan & Gong, 2008; Sahu, Maiti, Maiti, Ghosh, & Pramanik, 2010). It demonstrated ion sensitivity in aqueous solutions at different pH due to abundant carboxyl (–COOH) and amine ($-NH_2$) groups. Here, the carboxylate ($-COO^-$) anions present on CMC are conjugated with the surface of MNPs. The amine groups on the NPs surface are further conjugated with acrylic acid for increasing the carboxylic groups. The

* Corresponding author. Tel.: +91 9475196288; fax: +91 3222 25530.
E-mail address: sumantchem@gmail.com (P. Pramanik).

0144-8617/$ – see front matter © 2011 Elsevier Ltd. All rights reserved.
doi:10.1016/j.carbpol.2011.11.033

cancer cell targeting folate is conjugated onto the MNPs by 2,2′-(ethylene dioxy) bis(ethylamine) (EDBE) groups to target the cancer cells that have over-expressed folate receptors on their cell surface.

The method for preparation of MNPs coated with a shell containing luminescent organic dyes (rhodamine-B-isothiocyanate (RITC)) and therapeutic agent for cancers (Doxorubicin (DOX)) is developed. The DOX is accumulated inside the cell nucleus where it intercalates into DNA and interacts with *topoisomerase II* that become a cause for DNA cleavage and cytotoxicity (Zunino & Capranico, 1990). We would like to determine whether the fluorescence characteristics of the organic dye could be used in conjunction with florescence microscope to compare the efficiency of MNPs uptake into different cells. The cancer cells targeted with the multifunctional polymer NPs were detectable through both florescence microscopy and MRI. Scheme 1 introduces the ideal design for a highly versatile NP based core–shell system for addressing diagnostic and treatment requirements. This unique architecture enables therapeutic and imaging agents for targeted drug delivery. Recently, our lab has demonstrated multifunctional MNPs, designed with various phosphonic acid ligands, for the targeting of tumor cells, MRI sensitivity, and for therapeutic drug delivery (Das, Mishra, Maiti, Basak, & Pramanik, 2008; Das et al., 2009; Mohapatra, Mallick, Maiti, Ghosh, & Pramanik, 2007). In this study, we have developed a facile approach to surface modification of MNP by a polymeric system, replacing the ligand based functionalization.

Various research groups frequently use long-chain polymers and lipids for the stabilization of iron oxide NPs. Jain et al. reported a novel magnetic drug delivery system by incorporating pluronic (F-127) and oleic acid with iron oxide NPs prepared through the co-precipitation approach (Jain, Morales, Sahoo, Leslie-Pelecky, & Labhasetwar, 2005). Recently Lin et al. developed pluronic (F-127) modified water-soluble polyacrylic acid bound iron oxides NPs and conjugated with folic acid (Lin et al., 2009). However, there is a potential concern about the toxic effects of pluronic (F-127), towards human erythrocytes (Forster, Washington, & Davis, 1988), and increase of cholesterol and triglycerides level in the blood plasma (Wout et al., 1992). Chen et al. have reported temperature responsive magnetite/pluronic NPs (Chen et al., 2007), while Narain et al. have reported MNPs coated with poly (*N*-isopropylacrylamide) (PNIPAAm) (Narain, Gonzales, Hoffman, Stayton, & Krishnan, 2007). However, the main drawback of these thermosensitive polymers relates to their non-biodegradability as well as to the fact that thermal treatment is required for drug release, which is not always feasible for *in vivo* clinical applications. It is concluded from the above statements that a system can be easily prepared for required drug loading capacity, controlled release of the loaded drug and retention of the magnetic properties.

More specifically, here we present the design of the MNPs possessing all of the following advantages: (i) a reasonable size of the NPs carrier for anticancer drug; (ii) a high stability in physiological media; (iii) a chemotherapeutic agent Doxorubicin that is released from polymeric modified NPs through a pH-dependent mechanism; (iv) folate ligand is attached on the surface of the nanoparticles that can target tumor endothelial cells and subsequently induce receptor-mediated endocytosis for cell uptake; (v) a competitive drug loading capacity in comparison with other systems (with options to increase the loading capacity); (vi) synthesized MNPs for ultrasensitive MRI detection. An external localized magnetic field gradient may be applied to a chosen site to create a center of attention for the drug-loaded MNPs from blood circulation. The results indicate that the NPs have a high drug loading capacity and favorable release property for DOX. Transmission electron microscopy (TEM), dynamic light scattering (DLS), Fourier transmission infrared spectroscopy (FTIR), and vibrating sample magnetometer (VSM) were used to characterize the formulated MNPs for evaluation of particle size, chemical functionality, and magnetic properties, respectively. The facile synthesis of MNPs can be used for potential application as multifunctional agents for MR imaging and targeted drug delivery.

2. Experiment

2.1. Materials

Chitosan (weight average molecular weight (M_w) ~200 kDa), potassium persulfate ($K_2S_2O_8$), acrylic acid, ferric chloride ($FeCl_3$), ferrous sulphate ($FeSO_4$), EDBE, folic acid (FA), di-tert-butyldicarbonate (BoC_2O), dicyclohexyl carbodiimide (DCC), *N*-hydroxysuccinimide (NHS), 1-[3-(dimethylamino)propyl]-3-ethylcarbodiimide hydrochloride (EDC), trifluroacetic acid (CF_3COOH), RITC, trinitrobenzene sulfonic acid (TNBS), 4′-6-diamidino-2-phenylindole (DAPI), propidium iodide (PI), *RNase*, and 3-(4,5-dimethylthiazol-2-yl)-2,5-diphenyltetrazolium bromide (MTT) were purchased from Sigma–Aldrich Chemicals, USA. Commercially available dimethyl sulfoxide (DMSO) and *N*,*N*′-dimethyl formamide (DMF) were purified by vacuum distillation. Pyridine was purified by distillation over KOH. Monochloroacetic acid ($ClCH_2COOH$) and chloroform ($CHCl_3$) were procured from Merck, Germany. Fetal bovine serum and Minimum Essential Medium (MEM) were procured from Hyclone, USA and Himedia, India, respectively.

2.2. Preparation of MNPs and their surface modification

Superparamagnetic MNPs were prepared according to our previously reported procedure (Mohapatra et al., 2007). In a typical recipe, 0.324 g $FeCl_3$ and 0.274 g $FeSO_4{\cdot}7H_2O$ were taken in 40 ml deionized water under argon atmosphere. The solution was vigorously stirred and heated to 60–70 °C under an argon atmosphere. Subsequently 25% ammonia solution (ca. 5 ml) was injected into the flask and stirring was continued for another 30 min to allow the growth of the NPs. The solution was then cooled to room temperature and the resulting particles were subjected to magnetic decantation followed by repeated washing with distilled water followed by drying in a vacuum oven at 70 °C. The surface modification of resulting Fe_3O_4 NPs was carried out by the CMC and subsequent covalent binding onto Fe_3O_4 NPs without any activating agent. 1 g chitosan, 1.5 g sodium hydroxide and 20 ml mixture of water and isopropanal (1:9) into a flask (100 ml) to swell and alkalize at a given temperature for 1 h for the synthesis of CMC. The temperature was maintained in a water bath. The monochloroacetic acid (1.6 g) was dissolved in isopropanol (3 ml), and added into the reaction mixture dropwise for 30 min and reacted for 4 h at the same temperature, then the reaction was stopped by adding 70% ethyl alcohol (25 ml). The solid was filtered and rinsed in 70–90% ethyl alcohol to desalt and dewater, and vacuum dried at room temperature. The resulted product was sodium salt CMC. Three sets of experiments are carried out for surface modification on the MNPs. In each case 100 mg of the MNPs was dispersed in 10 ml millipore water. The pH was adjusted to 8 by the addition of 0.1 M NaOH then the reaction mixture was ultrasonicated for 10 min. Ultrasonic treatments were administered at 75W using Sonicator 3000 (Misonix, Inc., Farmingdale, NY) equipped with a microprobe. After that, various amounts (0.2%, 0.5%, and 2% by w/v) of sodium salt CMC were added and the reaction mixture was again ultrasonicated for 20 min and stirred for 12 h. The product was recovered from the reaction mixture by a permanent magnet and then washed with water, producing Fe_3O_4-CMC.

For the further modification 75 mg of the CMC coated with MNPs (Fe_3O_4-CMC) was dispersed in 25 ml distilled water. After that,

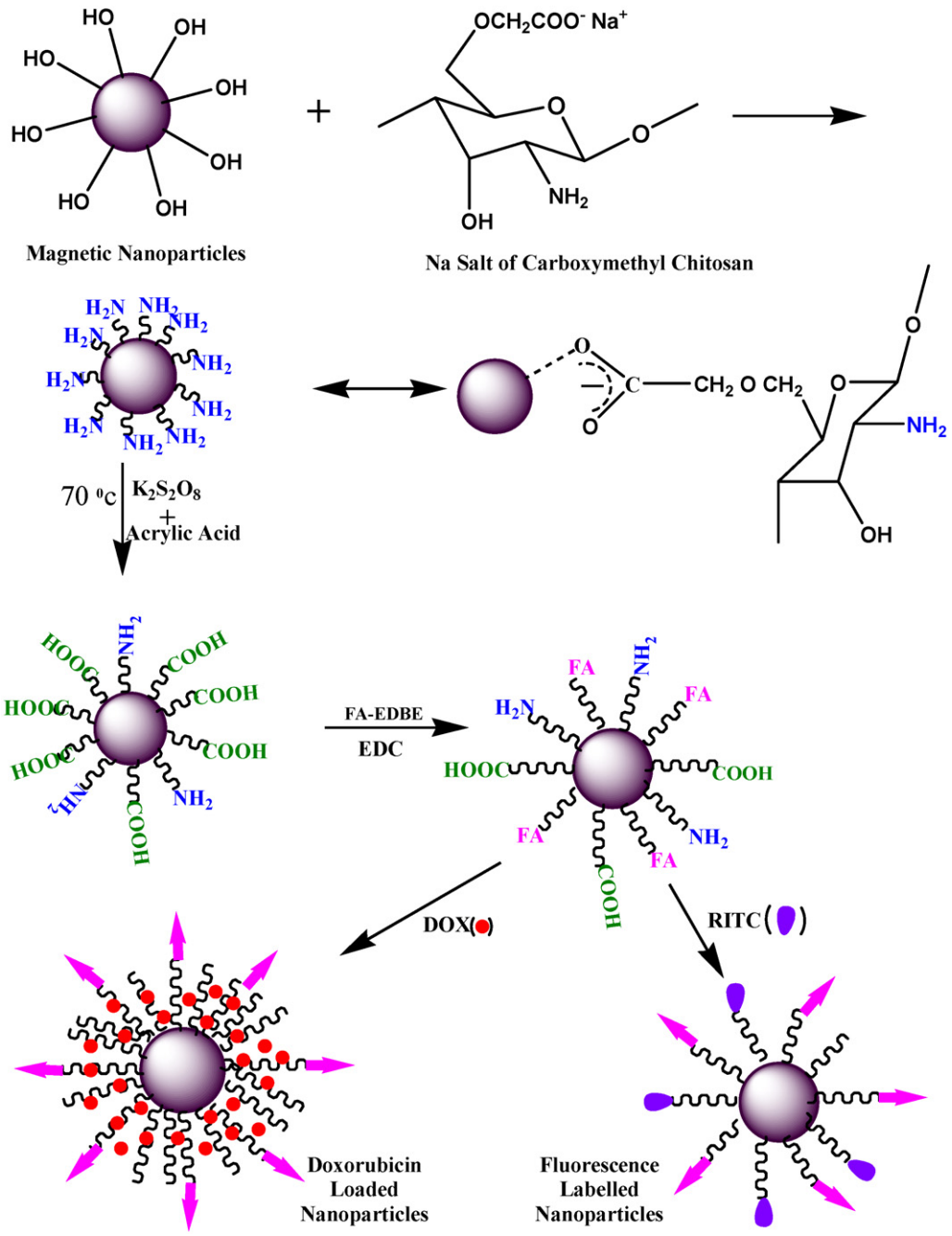

Scheme 1. Schematic illustration for the surface modification of MNPs by CMC and subsequent conjugation with folic acid, RITC, and doxorubicin.

MNPs reacted with acrylic acid (100 μl) in presence of $K_2S_2O_8$ under mechanical stirring at 70 °C for 2 h. After the reaction completed MNPs was recovered by permanent magnet and washed thoroughly with water, producing Fe_3O_4-CMC-AA.

2.3. Synthesis of γ-N-{2-[2-(2-aminoethoxy) ethoxy] ethyl} folic acid (FA-EDBE)

FA–EDBE was synthesized according to our previously reported method (Mohapatra et al., 2007). In brief, to a stirred solution of folic acid (0.75 mmol) in 20 ml anhydrous DMSO and pyridine (8 ml), dicyclohexyl carbodiimide (2 mmol), followed by tert-butyl *N*-{2-[2-(2-aminoethoxy) ethoxy] ethyl}-carbamate (0.87 mmol) was added. The reaction mixture was stirred for about 18 h at room temperature under argon atmosphere and the resulting precipitate was filtered. The filtrate was poured dropwise into a vigorously stirred cold solution of diethyl ether (Et_2O) at 0 °C. The yellow precipitate thus obtained was collected and washed several times with cold Et_2O to remove traces of DMSO. The solvent was then removed under reduced pressure to produce a yellow solid. CF_3COOH (2 ml) was added to the above product (0.65 mmol) at room temperature and allowed to stir. After 2 h, TFA was removed under reduced pressure and the resulting residue was dissolved in DMF. Then pyridine was added to initiate the formation of an orange-yellow precipitate. After complete precipitation, the resulting solid was washed with Et_2O and dried to afford FA-EDBE. ^{1}H NMR (DMSO-*d*6, 400 MHz): δ 2.5 (br s, β and γ-CH_2 groups superimposed, 4H), 2.9–3.5 (m, –CH_2– of EDBE, 12H), 4.3 (br s, NH_2, 2H), 4.5 (d, –NH–, 1H), 4 d at 6.5, 6.7, 7.6, 7.7 (benzene ring), 6.9 (s, aromatic H of pteridine), 8.7 (s, OH, 1H). Mass (ES+) 572 (MH+).

2.4. Surface modification of magnetite NPs with folate (Fe_3O_4-CMC-AA-FA)

Then the Fe_3O_4-CMC-AA particles were conjugated with folic acid through amidation between –COOH groups of NP and $–NH_2$ group of FA-EDBE.15 ml of Fe_3O_4-CMC-AA magnetite suspension (1 mg/ml) was sonicated for 10 min after that 10 ml aqueous solution of NHS (60 mg) and 25 mg of EDC was mixed and stirred for 2 h at 1000 rpm under mechanical stirring. Then 25 mg of FA-EDBE was added and the reaction was continued for 8 h. The magnetic suspension particles were recovered using a magnetic concentrator and washed with millipore water.

2.5. Quantification of amine and acid number on the NP surface

TNBS assay was used to determine the percentage of primary amines in the NPs solution (Morris & Sharma, 2010). The functionalized MNPs were dispersed with 4% sodium bicarbonate solution (pH 8.5). The dispersed MNP solution (2 ml) was added to 2 ml TNBS solution (0.1% w/v). After incubation for 1 h at 40 °C, NPs were isolated from the supernatant by magnetic concentration. The supernatant (1 ml) was added to an aqueous solution of glycine (0.1 ml, 40 mmol ml^{-1}) followed by incubation at 40 °C for 1 h to calculate the unreacted TNBS. After incubation the reaction was stopped by the addition of 1 ml of 2 N HCl, and the sample was subsequently hydrolyzed for 20 min at 40 °C. The absorbance was read at 410 nm using Shimadzu UV-1700 spectrophotometer. The $–NH_2$ group concentration was calculated by means of a graph originated by taking glycine (0–2 mmol) as standard. The free –COOH groups present on the surface of MNPs were quantified by titrating the dispersed MNP solution against NaOH (0.0005 N) to determine the acid numbers. The NaOH solution used was standardized by titrating against oxalic acid. Acid number was calculated by the following formula.

$$\text{acid number} = \frac{\text{volume required during titration} \times \text{normality of NaOH} \times 40\ (\text{Mol. Wt. of NaOH})}{\text{weight of NPs}}$$

2.6. Fluorescence labeled NPs

1 mg of RITC was dissolved in 5 ml of H_2O and added dropwise to an aqueous suspension of functionalized magnetite NPs (Fe_3O_4-CMC-AA-FA) at pH 8. The resulting suspension was sonicated for an hour in the dark and stirred for 6 h. Then particles were recovered by magnetic decantation and washed thoroughly with deionized water for three times to remove the unreacted RITC. Finally, the obtained RITC labeled NPs were dispersed in PBS solution for the *in vitro* experiment.

2.7. Cell lines and cytotoxicity study

The cells cultivated for *in vitro* experiments were human cervix adeno carcinoma (HeLa) cell lines and NIH3T3 (murine fibroblast) obtained from the national centre for cell sciences (NCCS), Pune, India and grown in MEM and Dulbecco's Modified Eagle's medium (DMEM) medium respectively with 10% fetal calf serum, penicillin (100 units/ml), streptomycin (100 mg/ml), and 4 mM L-glutamine at 37 °C in a 5% CO_2 and 95% air humidified atmosphere. Cells were harvested and the concentration was adjusted to 1×10^5 cells/ml. Cells were plated (180 μl/well) in a 96 well flat bottom culture plates and incubated with various concentrations of NP. Cells were incubated with and without DOX loaded NPs at 37 °C in a humidified incubator, which maintained a constant 5% CO_2. Cytotoxicity was estimated by MTT assay.

2.8. Intracellular uptake studies

The NP was labeled with RITC and incubated with cells at a concentration of 5 μg/ml for 1 h, 2 h and 4 h respectively to determine the NP uptake in HeLa cells. After incubation, cells were fixed with 42% paraformaldehyde for 15 min and stained with DAPI (1 mg/ml) for 5 min at 37 °C. Then cells were washed with PBS and examined under Olympus IX 70 fluorescence microscopy.

2.9. Cell cycle analysis

For cell-cycle analysis, HeLa cells (1×10^5) were treated with different concentration (1, 5, and 10 μg) of DOX loaded NP for 24 h at 37 °C. The cells were harvested and fixed in 70% ethanol stored at −20 °C. Then, the cells were washed with ice-cold PBS (10 mM, pH 7.4) and resuspended in 200 μl of PBS followed by incubation with 20 μl *DNAase* free *RNase* (10 mg/ml) and 20 μl of DNA intercalating dye PI (1 mg/ml) at 37 °C for 1 h in dark. Apoptotic cells were determined by their hypochromic sub-diploid staining profiles. The distribution of cells in the different cell-cycle phases was analyzed from the DNA histogram using a Becton–Dickinson FACS caliber flow cytometer and Cell Quest software.

2.10. Doxorubicin loading and release study

In this investigation, DOX was used as a model drug to estimate the loading and release patterns of the NPs. The NPs were washed with phosphate-buffered saline (pH 7.4), followed by a wash with deionized water. DOX was dissolved in the pH 6 buffer solution in advance and loaded onto NPs by exposing NPs to the DOX solution for 12 h. Then the magnetic nanoparticles were separated from the aqueous suspension medium by permanent magnet and followed by washing with water. The DOX can diffuse into the NPs in the pH 6 buffer solution because of change of the polymeric layer on the MNP charges upon this pH solution, loosening the layer networks. Therein a high concentration of drug molecules penetrates into the shell of the NPs. The quantitative estimation of the DOX loading was obtained by a UV–Vis spectrophotometer. DOX concentration was determined by measuring absorbance at 480 nm using a DOX calibration curve. Loading was expressed as the weight ratio of loaded DOX to NPs and encapsulation efficiency (EE) as the weight ratio of encapsulated DOX to total DOX used for encapsulation. The release of DOX from the NPs was determined by a spectroscopic method. The effect of the pH change on the release profile was also monitored.

2.11. MR imaging of cells labeled with folic acid modified MNPs

A clinical 1.5 T MR scanner (Sigma, GE Medical System, USA) was used to measure T_2-weighted signal intensities (SI). FR(+)HeLa cells and FR(−)NIH3T3 cells (1×10^5 cells) were seeded into a 12-well culture plate before adding the various concentrations of Fe_3O_4-CMC-AA and Fe_3O_4-CMC-AA-FA. The addition of the samples was followed by incubation at 37 °C for 2 h. The medium was dispensed and the cells were washed three times with 0.1 M PBS containing 2% FBS. The A repetition time (TR) of 2100 ms and variable echo times (TE) of 95–150 ms were used. T_2-weighted images were acquired using the following parameters, an acquisition matrix of 256 × 256, field of view of 240 mm × 240 mm, section thickness of 2 mm and two averages.

3. Results and discussion

3.1. Synthesis and design of MNP encapsulated polymeric shell for targeted delivery

Generally, the direct immobilization of a polymer with few reactive functional groups such as chitosan to magnetite NPs could not be easily achieved. Here, CMC is selected as one of the magnetic carriers. Monodispersed superparamagnetic MNPs are first synthesized by chemical co-precipitation method and the hydroxyl groups on its surfaces were exchanged with $–COO^-$ groups to make the surface modified MNPs. The amphoteric polyelectrolyte, sodium salt of CMC has demonstrated ion sensitivity in aqueous solutions due to abundant $–COO^-$ and $–NH_2$ groups. The development of adsorption of charged macromolecules has emerged as a promising approach to fabricate controlled and highly ordered molecular assemblies on the NPs surfaces. The strategy involves the construction of polyelectrolyte multi-layers on the surfaces of NPs. The electrostatic interactions between oppositely charged polyelectrolytes create a multi-layer polymer of nanometer scale thickness. Here, we extended the method to MNPs to produce a new class of core–shell particles. These multi-layered polyelectrolytes are of particular interest because of their inherently high surface area. The electrostatics or hydrogen bonding plays a significant role for formation of layers. However, the layer formation on the NPs surface was dependent on increasing the quantities of CMC. During coating of CMC to the magnetic nanoparticles, CMC gets chemisorbed on the surface of the magnetic nanoparticles. The hydrophilic nature of the CMC makes the CMC coated magnetic particles easily dispersible in the aqueous solutions. For the utilization of nanoparticles for drug delivery purpose, it is better to have a water dispersible formulation. To get a desirable amount drug loading, the different quantity of CMC has to be coated the surface of the MNPs. Therefore, particles were synthesized by increasing concentration of CMC. Fig. 1(A)–(C) shows the TEM images of the CMC modified MNPs at CMC concentration of 0.2%, 0.5%, and 2% by w/v, respectively. The histograms of right-hand side each image represent the corresponding DLS diameters of the CMC modified Fe_3O_4 particle. It can be seen that the distribution of Fe_3O_4 within the polymer matrix is not significantly affected by the increase in the polymer concentration. However, the size of the Fe_3O_4-CMC was increased with increase in CMC concentration at the fixed iron oxides loading. This is understandable since more polymer molecules could cover larger surfaces of the NPs. The TEM observation indicates that there is occurrence of low fraction of monolayer coverage on the MNPs surface at 0.2% CMC solution. Thicknesses of 6–8 nm were measured for each subsequently deposited polyelectrolyte layer comprising up to 2% CMC solution. It was found that the layer could be successfully deposited by polyelectrolyte, leading to formation of core–shell NPs. The hydrodynamic particle size of whole NPs (inclusive of the polymer shell and the magnetite core) was determined by DLS measurement to further support the TEM results (provide information on the size of the Fe_3O_4 core). The DLS measurements revealed that the CMC grafted MNPs obtained from the above mentioned possess are relatively narrow size distribution. The detail size variation of the functionalized magnetic nanoparticles prepared in different concentrations of CMC is summarized in Table 1. DLS measurements are expected to give the hydrodynamic radius rather than the actual size of the nanoparticles. A measurement of the hydrodynamic radius of the nanoparticles would account for the larger DLS measurement than the TEM images because the CMC is expected to have a much smaller configuration dried on the TEM grid. When we have used 2% CMC, nanoparticles seem to be aggregate together. However, it is well known that by TEM we image some part of the grid, while DLS gives an average size estimation, which is biased towards the larger-size end of the population distribution. In all cases the polydispersity index value was less than 0.2. It is revealed that the overall volume of the NP system is significantly increased with increase in polymer concentrations. These results show that the method is an excellent technique for preparation of monodispersed core–shell NPs.

Table 1
Size variation of the functionalized magnetic nanoparticles dispersed in different % concentrations of Na salt of CMC (w/v).

Sample	% CMC used	Hydrodynamic diameter (nm)	TEM (nm)
Fe_3O_4-CMC (0.2%)	0.2	58 ± 12	20 ± 2
Fe_3O_4-CMC (0.5%)	0.5	70 ± 10	22 ± 4
Fe_3O_4-CMC (2%)	2	94 ± 15	25 ± 5

In the present work we have synthesized FA-functionalized MNPs as tumor selective targeting agents. The poor solubility of folic acid in aqueous medium provides the possibility to conjugate it with a hydrophilic linker (EDBE) by using DCC. This FA-EDBE is easily soluble in aqueous medium. After CMC modification on the NPs surface, there are no more carboxyl groups to conjugate with FA-EDBE. The CMC-MNPs is decorated with acrylic acid for enhancement of the carboxyl groups on its surface. The surfaces of the MNPs are grafted by copolymerization reaction of the primary amine ($–NH_2$) with vinyl monomers of acrylic acid in presence of $K_2S_2O_8$. This is a crucial step for the encapsulation of MNPs with acrylic acid. Here $K_2S_2O_8$ has been used to initiate the graft copolymerization with amines group of chitosan and vinyl monomers of acrylic acid (Qian, Cui, Ding, Tang, & Yin, 2006; Sun, Xu, Liu, Xue, & Xie, 2003; Xie, Xu, & Wang, 2002). There was maximum probability of conjugation between the amine groups and carboxyl groups, through activated persulfate with Fe_3O_4-CMC NPs then added acrylic acid. After conjugation of acrylic acid the –COOH groups of the MNP surface were conjugated to the FA-EDBE through covalent interactions using EDC. The nanoparticles contain –COOH and also amino groups. For the attachment of the derivative of folic acid (FA-EDBE) by carbodiimide method it may be lead to the inter and intra- crosslinking of nanoparticles due to the reaction of –COOH and NH_2 groups of nanoparticles. But we did not observe such type of agglomeration. The excess –COOH groups of acrylic acid may be present at the inner layer and it provides interaction with guest molecules of the drugs. The numbers of amine and acid groups are quantified by TNBS assay and acid-base titration method, respectively for encapsulation of RITC and DOX molecules.

3.2. FT-IR analysis

The surface functional groups were characterized by FT-IR. The FTIR spectra of pure Fe_3O_4, CMC modified Fe_3O_4 NPs, and AA conjugated CMC modified Fe_3O_4 NPs are displayed in Fig. 2 together with the FTIR spectra of pure FA and Fe_3O_4-CMC-AA immobilized FA. The spectrum of CMC conjugated Fe_3O_4 NPs show not only the main characteristic band of the naked pure Fe_3O_4 NPs at 590 cm^{-1} but also the characteristic peaks of CMC at 1583 cm^{-1} (corresponding to the amino groups), 3420 cm^{-1} (O–H stretching and N–H stretching vibrations), 1645, 1548 cm^{-1} (amide I and amide II of amino group) and 1076 cm^{-1} (C–O–C stretching vibration), which are consistent with the previous publications (Bahadur, Lee, Yoo, Choi, & Ghim, 2009; Belessi et al., 2008). The carboxylate ion of the CMC is coordinated with the MNPs as a chelating ligand (Okassa et al., 2007; Zhang, He, & Gu, 2006) and amines groups are on the surface. After conjugation with acrylic acid, the spectrum of the resultant NPs (Fe_3O_4-CMC-AA) shows not only the characteristic bands of the original Fe_3O_4-CMC NPs at 590, and 1583 cm^{-1} but also the characteristic peaks at 1741 cm^{-1} corresponding to the –COOH groups, which will subsequently takes part in folic acid conjugation through

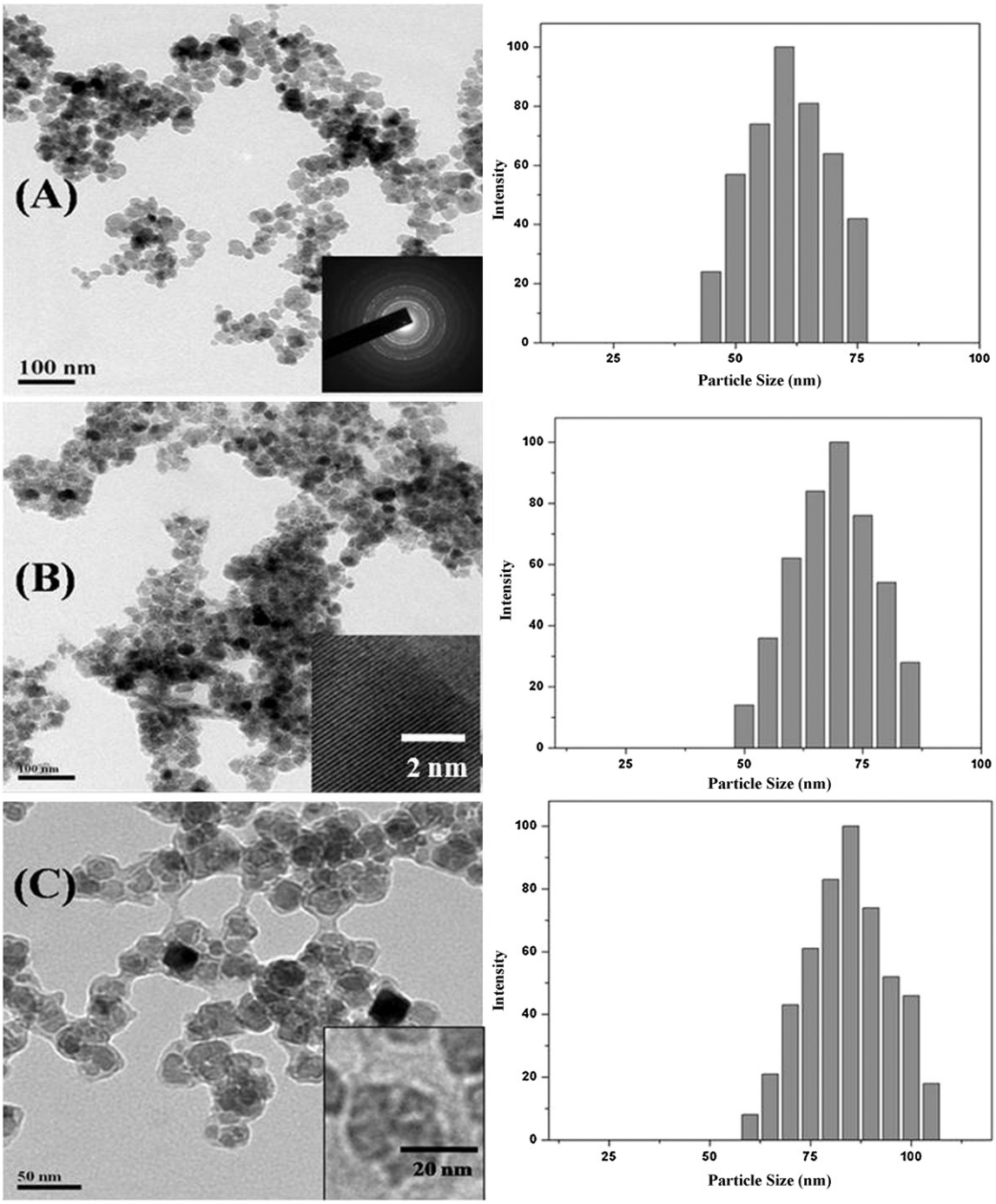

Fig. 1. TEM images and size distribution of MNPs embedded in the (A) 0.2% CMC (inset – diffraction pattern of CMC-MNPs), (B) 0.5% CMC (inset – high-resolution TEM image showing the crystalline condition of iron oxide), and (C) 2% CMC (inset – iron oxide NPs were encapsulated in the CMC shell) conjugated on the surface in aqueous solution.

EDBE. The FTIR spectrum of the FA standard presents characteristic bands at 3545, 3324, 2960, 2924, 1694, 1640, 1603, 1484, and 1412 cm^{-1}. Similarly, the amide carbonyl bands correspond to 1635 and 1556 cm^{-1} stretching vibrations are intensified in the spectrum of Fe_3O_4-CMC-AA-FA because of the immobilization of FA-EDBE on the carboxyl-terminated NPs. The characteristic absorption bands of folic acid are also observed at reduced intensity due to the small concentration on the surface of Fe_3O_4-CMC-AA-FA. The characteristic band at 1459 cm^{-1} corresponds to the phenyl ring of folic acid and the other bands are also identified in the spectrum confirms the successful conjugation of folic acid on the NPs.

3.3. Hysteresis and XRD studies

Fig. 3(A) shows the hysteretic M–H curves of the MNPs prepared by the precipitation method at the various emulsifier concentrations. The normalized saturation magnetization of the bare Fe_3O_4 crystals is 62.5 emu/g while that of the Fe_3O_4-CMC are 56.4, 51.7 and 41.66 emu/g when prepared at the 0.2%, 0.5%, and 2% by w/v concentration, respectively. The saturation magnetization values of the Fe_3O_4-CMC are found to be always lower than that of bare Fe_3O_4 crystals due to the encapsulation within the non-magnetic polymer matrix (Hamoudeh et al., 2007). Moreover, the

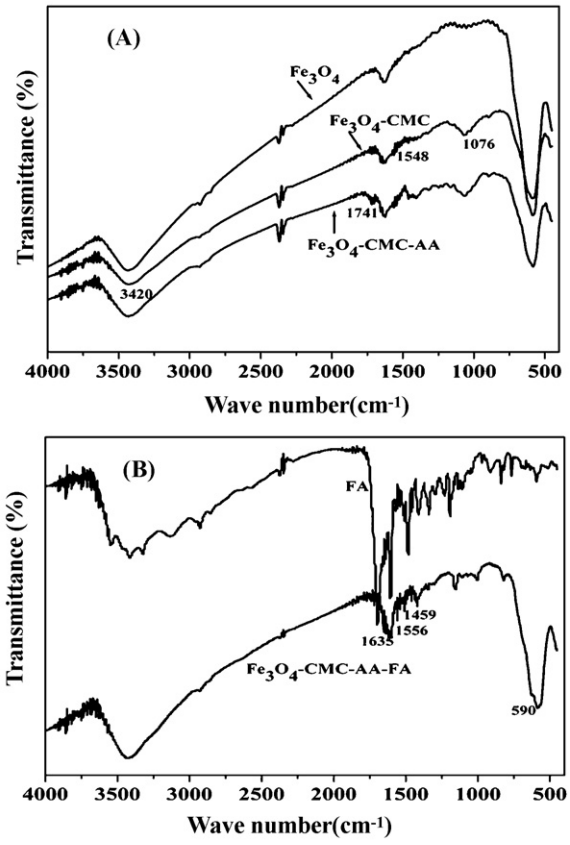

Fig. 2. (A) FTIR spectra of MNPs, CMC coated MNPs, acrylic acid conjugated on CMC coated MNPs (Fe_3O_4-CMC-AA) and (B) FTIR spectra of folic acid, folic acid conjugated Fe_3O_4-CMC-AA.

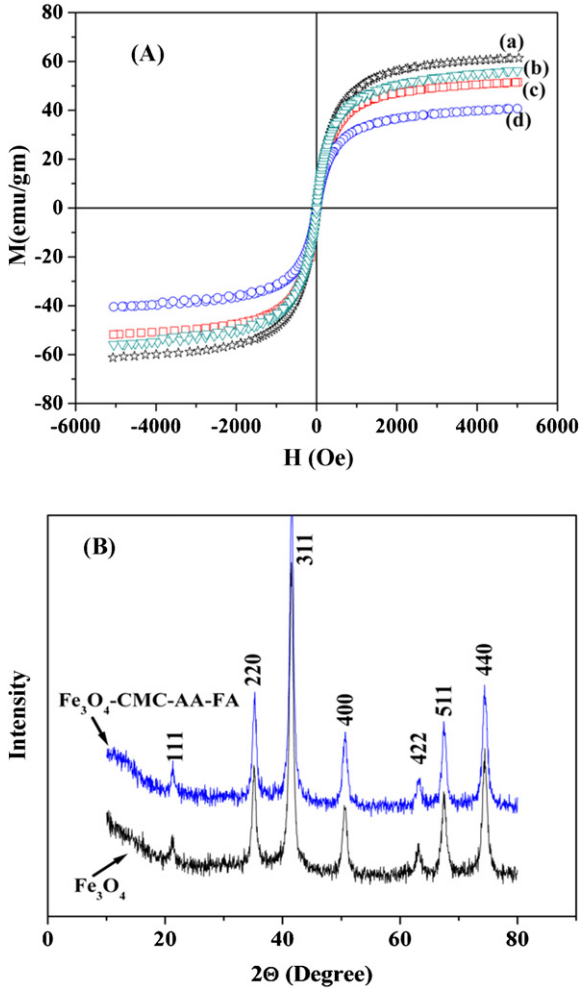

Fig. 3. (A) Plots of magnetization versus magnetic field at 300 K for (a) pure MNPs, (b) 0.2% CMC, (c) 0.5% CMC, and (d) 2% CMC encapsulated MNPs and (B) X-ray diffraction patterns for pure Fe_3O_4 NPs and Fe_3O_4-CMC-AA-FA functionalized Fe_3O_4NPs.

saturation magnetization values of the Fe_3O_4-CMC are found to decrease on increasing the CMC concentration in the NPs modification process. The difference in magnetization value between bare Fe_3O_4 NPs and Fe_3O_4-CMC particles can be attributed to the nonmagnetic organic components which can reduce the total magnetization to a different extent. The zero coercivity and remenance of the M∼H curves indicate that all of the encapsulated Fe_3O_4 NPs are superparamagnetic in nature. There is no obvious loss of saturation magnetization was observed after folic acid conjugation compared with that of Fe_3O_4-CMC MNPs (not shown in figure).

Powder XRD analysis exhibits the characteristics of the crystallographic structure and physical properties of the materials shown in Fig. 3(B). The pure Fe_3O_4 and Fe_3O_4-CMC-AA-FA NPs show identical characteristic diffraction peaks at $2\theta = 30.1^\circ, 35.5^\circ, 43.1^\circ, 53.4^\circ, 57.0^\circ$, and 62.6° corresponds to the reflection plane indices of (2 2 0), (3 1 1), (4 0 0), (4 2 2), (5 1 1) and (4 4 0), respectively. This reveals that the surface modification and conjugation of the Fe_3O_4 NPs do not lead to their phase change.

3.4. In vitro cytotoxicity

The *in vitro* cytotoxicity of Fe_3O_4-CMC-AA-FA NPs and DOX loaded Fe_3O_4-CMC-AA-FA-DOX NPs are demonstrated by cell viability through the MTT assay using the HeLa and NIH3T3 cell line. It is established that the folic acid modified NP has greater cytotoxic effect towards HeLa cells as compare to the normal cell and folate receptor deficient cell lines *in vitro* due to the folate-mediated targeting properties (Sahu, Maiti, Maiti, Ghosh, & Pramanik, 2011). The role of folate decorated NP in HeLa and NIH3T3 cell lines is investigated for better comparison of folate receptor (FR) over expression of HeLa cells and FR deficiency of NIH3T3 cell lines (Leamon & Low, 1994). The Fe_3O_4-CMC-AA-FA-DOX NPs showed a significant growth inhibition for HeLa cells in a dose dependent manner in comparison to NIH3T3 cells (Fig. 4). The 50% inhibition concentration (IC_{50}) value of (Fe_3O_4-CMC-AA-FA-DOX) NP was 3 μg/ml in HeLa cells and 22 μg/ml in NIH3T3 cells. On the other hand, without DOX loaded NPs have not shown this much inhibition up to 25 μg/ml towards both HeLa and NIH3T3 cells.

3.5. Intracellular uptake of NPs

HeLa and NIH3T3 cells were treated with RITC-NP at a concentration of 5 μg/mL for 1 h, 2 h, and 4 h and were observed under fluorescence microscope to determine folate decorated NP internalization and cytoplasmic distribution. Fig. 5 shows that NPs were distributed in the cytoplasm proximity to the cell membrane up to 60 min after treatment in HeLa cells. Initially, RITC-NP in HeLa cells are localized to the cell membrane and then moved from the membrane intra-cellularly with time, which indicated cellular uptake and/or internalization of the NP in HeLa cell by folate receptor. The internalization of NP in NIH3T3 cells are not observed that suggests the cancer specificity nature of the folate decorated NP.

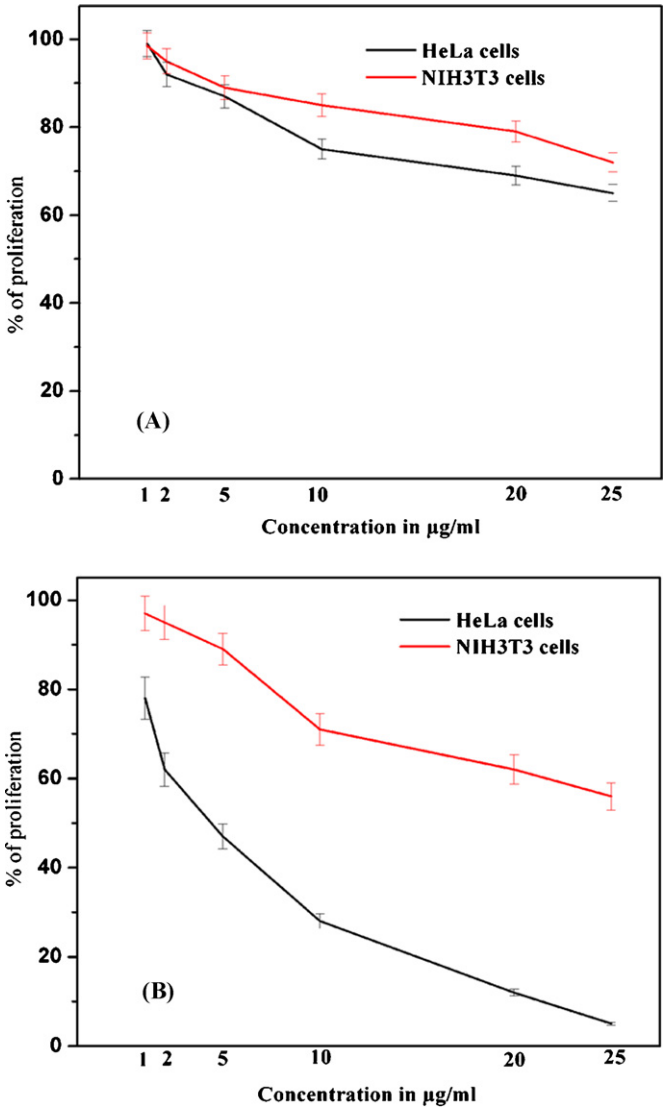

Fig. 4. Cell viability of (A) HeLa cells and NIH3T3 cells treated with Fe_3O_4-CMC-AA-FA NPs at different concentrations and (B) HeLa cells and NIH3T3 cells treated with Dox loaded Fe_3O_4-CMC-AA-FA NPs at different concentrations. Cells were incubated with NPs for 24 h.

3.6. Cell cycle analysis

The cell viability of the HeLa cells are decreased, which may be mediated through apoptosis induction and inhibition of cell cycle. The literature survey indicates that the DOX is widely used as anticancer agent as it prevents cancer cell growth by inducing DNA breakage as well as cell cycle arrest (Zheng et al., 2009). It arrests cell cycle at G2/M phase (Ling, Naggar, Priebe, & Perez-Soler, 1996). It is observed that both SubG0/G1 and G2/M phases increased in DOX loaded NP treated cells with respect to control at 24 h of incubation of HeLa cells as shown in Fig. 6. The SubG0/G1 or the apoptotic cells found to be 3.5%, 6.2%, 8.1%, and 11.4% in control, 1, 5, and 10 μg/ml DOX treated cells, respectively. This result suggested that DOX loaded NP caused apoptosis in HeLa cells. Similarly, the G2/M phase is found to be 14.2% 16.7%, 20.5%, and 36.7% in control and 1, 5, and 10 μg/ml treated groups, respectively. On other hand, the G0/G1 phase is decreased in dose depended way without a significant alternation in S phase of DOX loaded NP groups. These results suggested that DOX loaded NP inhibited the growth of HeLa cells by arresting cell-cycle progression at G2/M and followed to apoptosis.

Table 2
Encapsulation of free doxorubicin within the polymeric shell of magnetic nanoparticles.

Nanoparticle	Initial loading (%) (w/w)	Loading content (%) (w/w)	Loading efficiency (%) (w/w)
Fe_3O_4-CMC (0.2%)-AA-FA	14	2.9	20.71
	32	6.74	20.75
	48	13.24	27.58
Fe_3O_4-CMC (2%)-AA-FA	14	11.8	79.14
	32	25.1	78.53
	48	37.16	77.41

Initial loading is a weight ratio of initially added free doxorubicin to nanoparticles.
drug loading contents (%) $= \frac{\text{weight of drug in nanoparticles}}{\text{weight of prepared nanoparticles}} \times 100$
drug entrapment efficiency (%) $= \frac{\text{weight of durg in nanoparticles}}{\text{weight of drug injected}} \times 100$

3.7. In vitro drug release

The design of new class nanofabricated systems is greatly expected for target drugs delivery. However, these magnetic particles may possess more obvious advantages as drug delivery systems in comparison to the existed magnetic nanomaterials. The drug loading capacity is investigated by taking DOX as anticancer agent to assess the potential of the NPs as drug delivery vehicles. The NPs were loaded with drug by mixing them with DOX solution. A water-soluble DOX is adsorbed on the shell of the NPs. The DOX molecules diffuse from the high concentration to low concentration that encapsulate into the shell of the NPs because of the diffusion effect. These DOX molecules inside the shell would interact with CMC to form complexes as a consequence more and more DOX molecule penetrates into the shell of NPs.

As listed in Table 2, the amount of DOX incorporated into the Fe_3O_4-CMC (2%)-AA-FA NPs (one day immersion) was ~4 times higher than that of the Fe_3O_4-CMC (0.2%)-AA-FA NPs. Actually, our modified MNPs exhibited higher DOX loading amounts, indicating that polymer layer existed on the surface of NPs probably plays an important role on loading DOX molecules. This result demonstrates the potential utility of NPs as efficient vehicles for targeted delivery of anticancer therapeutic agents through conjugation with targeting molecules. The increase in drug loading content and entrapment efficiency was due to the increase in surface area from the presence of CMC molecules on the surface of the MNPS. It could be hypothesized that the DOX molecules encapsulate into the shells of CMC molecules surrounding the NP surface. However, it should be noted that a relatively large amount of DOX could be physically loaded into the NPs in a more facile way, compared to other conventional polymeric modified MNPs.

The amount of DOX released from nanoparticles is investigated at different pH. It is observed all cases the burst release from the nanoparticles at an early period. Fig. 7 presented the DOX release study for Fe_3O_4-CMC (2%)-AA-FA nanoparticles. In the DOX release tests, approximately 52% of DOX from Fe_3O_4-CMC-AA-FA NPs was released within 24 h at pH 5.1 compared to approximately 21% at pH 7.4 (Fig. 7). The burst release from the nanoparticles at an early period was significant. The faster drug release rate in lower pH medium could be contributed to two factors: the one is the loose nanoparticle structure, which caused by the stronger protonation of the free amino groups of chitosan in lower pH; the other is the higher solubility of DOX in lower pH. So the drug release rate from nanoparticles reduced with the increase of the pH value of dissolution medium. These NPs were suitable for systemic application and were released more in acidic pH than in normal physiological condition. It is assumed that the DOX release would be quicker in a mildly acidic tumor environment than in normal tissue or blood due to the weak binding between DOX and the carboxylic groups of the polymer and the reprotonation of the amino groups

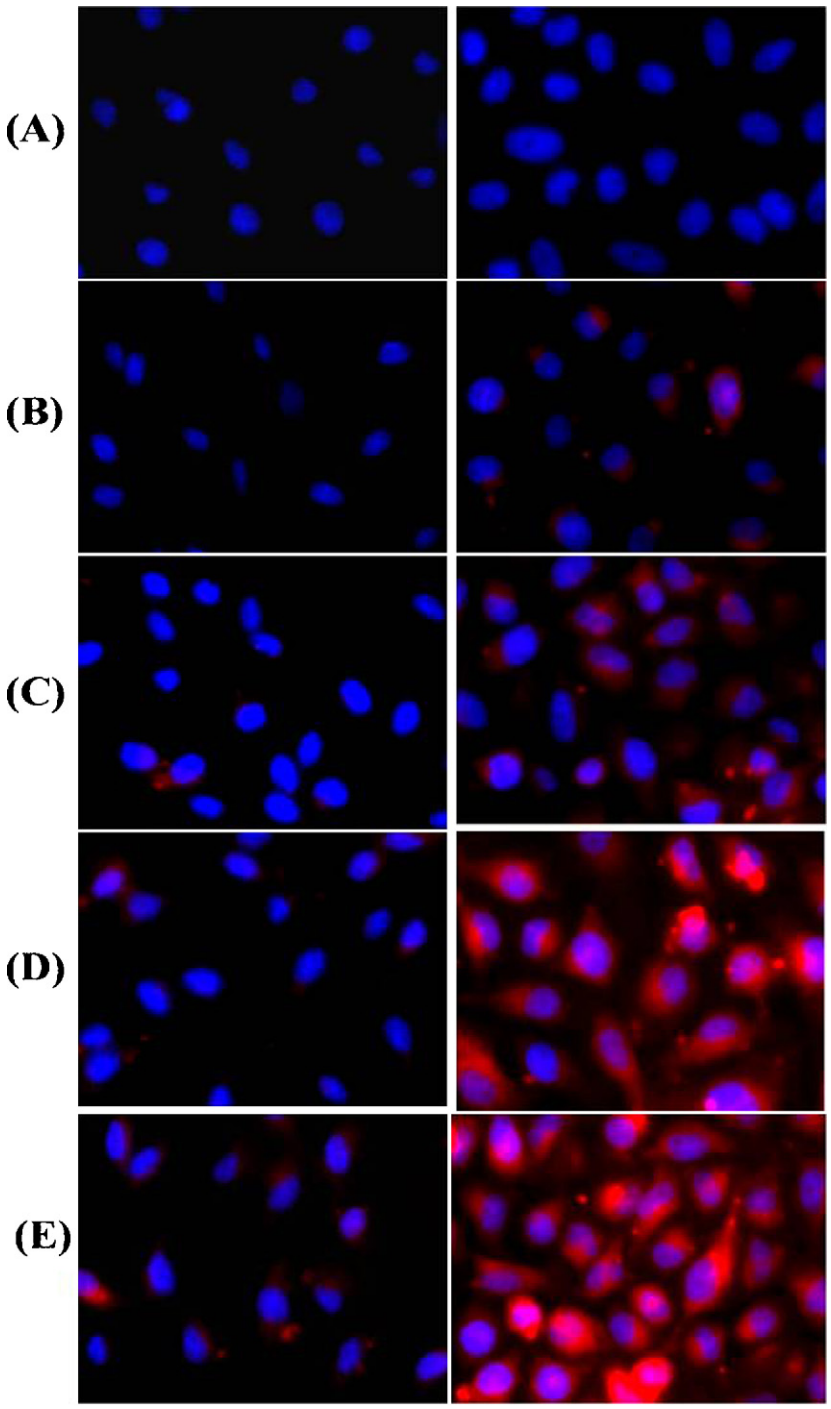

Fig. 5. Florescence microscopic pictures of uptake of NP NIH 3T3 cells (left) and HeLa cells (right) incubated with Fe_3O_4-CMC-AA-FA NPs after (A) 0 h incubation, (B) 0.5 h incubation, (C) 1 h incubation, (D) 2 h incubation, and (E) 4 h incubation.

of DOX. Moreover, NPs are usually internalized inside the cells by endocytosis. Accordingly, more accelerated release inside the endosome/lysosome of tumor cells may occur due to the decreased pH values. Therefore, this pH-dependent release function is especially useful for achieving the tumor-targeted drug delivery with NPs. Also, Fe_3O_4-CMC-AA-FA NPs were stable in water without noticeable degradation or aggregation over a several months (data not shown). The interesting loading and release behaviors of DOX from NPs will probably make them be used as an effective functional material for magnet controlled simultaneous cancer imaging and therapy *in vivo*, which is very important in the field of biomedicine.

3.8. MRI study

To estimate the utility of Fe_3O_4-CMC (2%)-AA-FA nanoparticles as an MRI contrast agent, the SI were measured using a 1.5-T MRI system. *In vitro* MR imaging was performed using similar conditions as in the cellular uptake experiments. The cellular uptake images of the folate decorated MNP into FR(+)HeLa cells and FR(−)3T3cells visualized by MRI (Fig. 8) and were performed under similar conditions as in the aforementioned florescence experiments. This was done to estimate the potential of Fe_3O_4-CMC (2%)-AA-FA as targeted MR contrast agents to cancer cells that over express

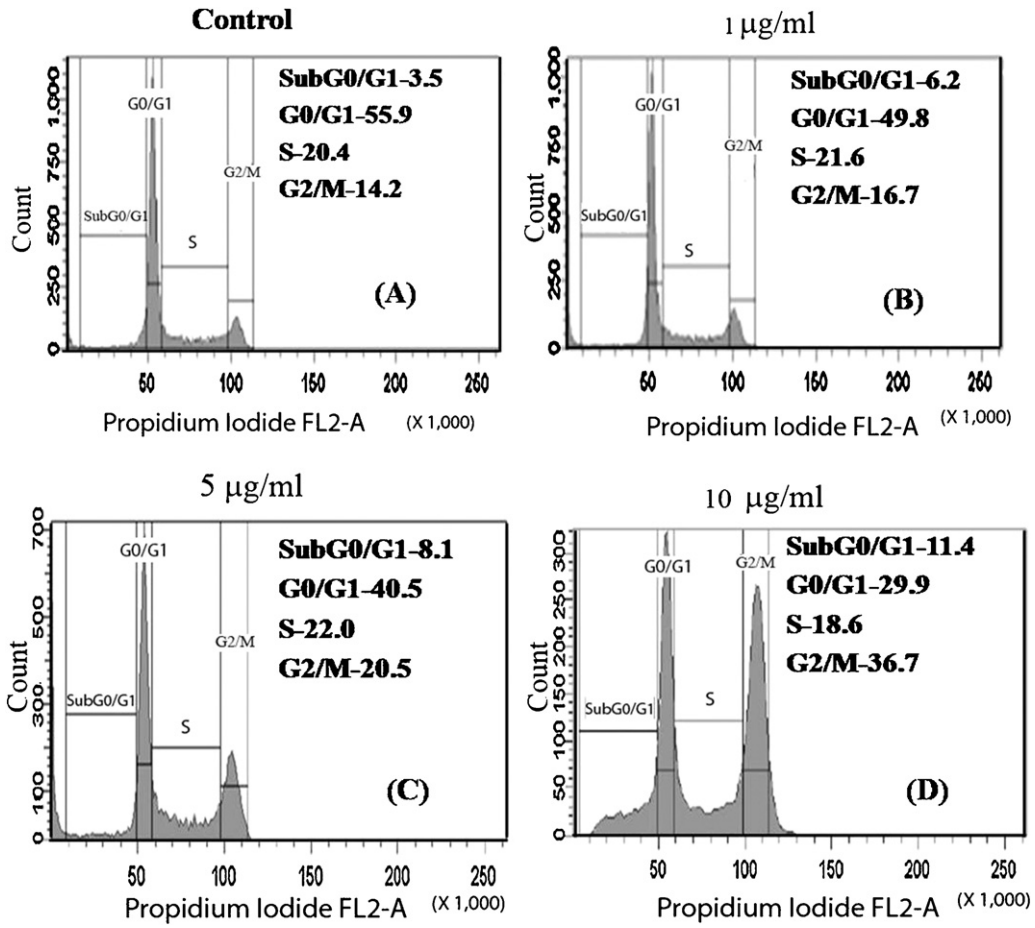

Fig. 6. Flow-cytometric analysis of cell cycle phase distribution. Distribution of HeLa cells treated with (A) PBS, (B) 1 μg/ml, (C) 5 μg/ml, and (D) 10 μg/ml of Dox loaded NP for 24 h was determined by flow cytometry using FACS Diva software after the cells were labeled by PI preceding RNAase treatment and percentage of apoptosis was calculated.

folate receptors. FR(+)HeLa cells and FR(−)3T3cells cultured with Fe_3O_4-CMC (2%)-AA-FA or Fe_3O_4-CMC (2%)-AA at various iron concentrations were incubated for 4 h at 37 °C. The images of the cells incubated with Fe_3O_4-CMC (2%)-AA-FA displays a better negative contrast enhancement (signal darkening) over those cells incubated with Fe_3O_4-CMC (2%)-AA. The T_2-weighted phantom image of cells incubated with folate-targeted NPs showed a significant

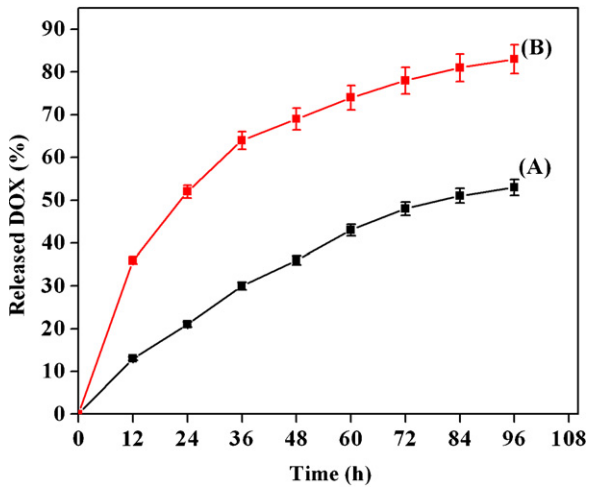

Fig. 7. *In vitro* doxorubicin releases from NPs at different pH solution (A) 7.2 and (B) 5.

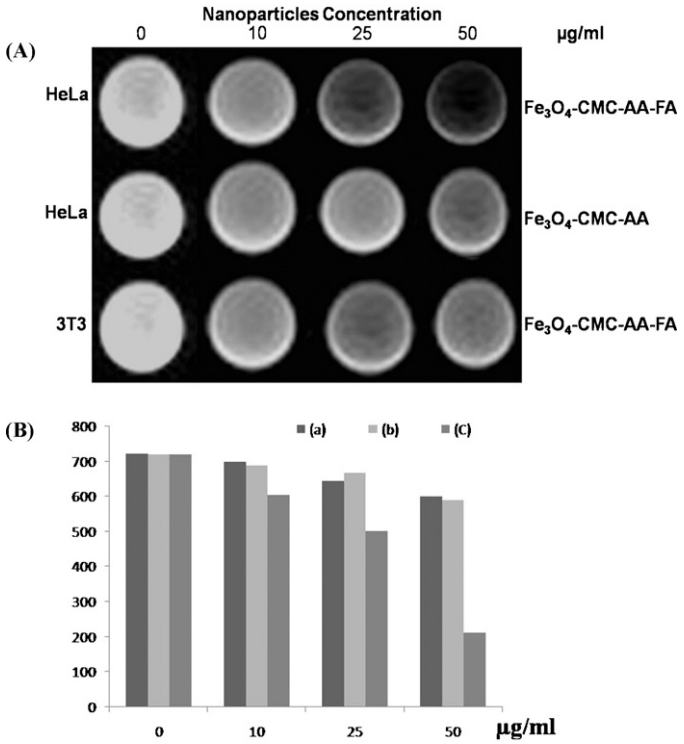

Fig. 8. (A) *In vitro* T_2-weighted spin-echo MR phantom images of NPs at different concentrations incubated in cell lines and (B) MR signal intensity of (a) Fe_3O_4-CMC-AA-FA NPs in NIH 3T3 cells, (b) Fe_3O_4-CMC-AA NPs in HeLa cells, and (c) Fe_3O_4-CMC-AA-FA NPs in HeLa cells incubated for 2 h.

negative contrast enhancement in comparison to its non targeted control, which suggested effective NP internalization inside the target cells. As shown in Fig. 8, the T_2 weighted images changed drastically in signal intensity with an increasing concentration of NPs, indicating that the synthesized NPs are potential T_2 contrast agents. This distinguishable darkening of MR images of the cells is due to folate receptor mediated endocytosis. The MRI SI of NPs decreased according to the iron concentration in the T_2-weighted images, and the SI of Fe_3O_4-CMC (2%)-AA-FA were about half of that of Fe_3O_4-CMC (2%)-AA in HeLa cells at the same iron concentration (2.5 mg/ml), even though Fe_3O_4-CMC (2%)-AA-FA has a higher SI in 3T3 cells (Fig. 8).

4. Conclusion

In a nut shell, the organic-dye-labeled Fe_3O_4-CMC-AA-FA (core–shell) MNPs have been prepared using modified CMC. The thickness of the polymer shell could be easily controlled by adjusting the ratio of MNP to CMC. The core–shell MNPs were also labeled with organic dye (RITC). The internalization efficiencies of the labeled NPs were investigated through *in vitro* cell studies. It is concluded that the core–shell MNPs may be applicable in biological labeling and in targeted drug delivery. In this context, these NPs which are able to carry high payloads of MR-active magnetic centers and they can take up a large amount of therapeutic drug within the shell surfaces are in attractive propositions. This study indicates that Fe_3O_4-CMC-AA-FA is able to provide a single nanoscale construct, which is capable of tumor cell-targeting, imaging, and drug delivery functions. To our knowledge, this is the first description of a chitosan based MNPs system possessing all of the above mentioned capabilities. This targeted delivery system may also provide a strategy for tumor cell detection and labeling applications *in vivo*.

Acknowledgements

The authors express gratefulness to the Department of Biotechnology, Government of India for funding and Indian Institute of Technology, Kharagpur for execution of these studies. Also Dr S.K. Sharma of ECO MRI Scan Centre, Kolkata, India is acknowledged for assistance with MRI studies.

References

Bahadur, K. C., Lee, S. M., Yoo, E. S., Choi, J. H., & Ghim, H. D. (2009). Glycoconjugated chitosan stabilized iron oxide nanoparticles as a multifunctional nanoprobe. *Materials Science and Engineering C*, *29*, 1668–1673.

Basti, H., Tahar, L. B., Smiri, L. S., Herbst, F., Vaulay, M., Chau, F., Ammara, S., & Benderbous, S. (2010). Catechol derivatives-coated Fe_3O_4 and γ-Fe_2O_3 nanoparticles as potential MRI contrast agents. *Journal of Colloid and Interface Science*, *341*, 248–254.

Belessi, V., Zboril, R., Tucek, J., Mashlan, M., Tzitzios, V., & Petridis, D. (2008). Ferrofluids from magnetic-chitosan hybrids. *Chemistry of Materials*, *20*, 3298–3305.

Chen, S., Li, Y., Guo, C., Wang, J., Ma, J., Liang, X., Yang, L. R., & Liu, H. Z. (2007). Temperature-responsive magnetite/PEO-PPO-PEO block copolymer nanoparticles for controlled drug targeting delivery. *Langmuir*, *23*, 12669–12676.

Das, M., Mishra, D., Dhak, P., Gupta, S., Maiti, T. K., Basak, A., & Pramanik, P. (2009). Biofunctionalized, phosphonate-grafted, ultrasmall iron oxide nanoparticles for combined targeted cancer therapy and multimodal imaging. *Small*, *5*, 2883–2893.

Das, M., Mishra, D., Maiti, T. K., Basak, A., & Pramanik, P. (2008). Bio-functionalization of magnetite nanoparticles using an aminophosphonic acid coupling agent: New, ultradispersed, iron-oxide folate nanoconjugates for cancer-specific targeting. *Nanotechnology*, *19*, 415101–415115.

Dilnawaz, F., Singh, A., Mohanty, C., & Sahoo, S. K. (2010). Dual drug loaded superparamagnetic iron oxide NPs for targeted cancer therapy. *Biomaterials*, *31*, 3694–3706.

Dobson, J. (2006). Magnetic nanoparticles for drug delivery. *Drug Development Research*, *67*, 55–60.

Fang, C., & Zhang, M. Q. (2009). Multifunctional magnetic nanoparticles for medical imaging applications. *Journal of Materials Chemistry*, *19*, 6258–6266.

Forster, D., Washington, C., & Davis, S. S. (1988). Toxicity of solubilized and colloidal amphotericin B formulations to human erythrocytes. *Journal of Pharmacy and Pharmacology*, *40*, 325–328.

Hafeli, U., Riffle, J. S., Harris-Shekhawat, L., Carmichael-Baranauskas, A., Mark, F., Dailey, J. P., & Bardenstein, D. (2009). Cell uptake and *in vitro* toxicity of magnetic nanoparticles suitable for drug delivery. *Molecular Pharmaceutics*, *6*, 1417–1428.

Hamoudeh, M., Faraj, A. A., Canet-Soulas, E., Bessueille, F., Leonard, D., & Fessi, H. (2007). Elaboration of PLLA-based superparamagnetic nanoparticles: Characterization, magnetic behaviour study and in vitro relaxivity evaluation. *International Journal of Pharmaceutics*, *338*, 248–257.

Jain, T. K., Morales, M. A., Sahoo, S. K., Leslie-Pelecky, D. L., & Labhasetwar, V. (2005). Iron oxide nanoparticles for sustained delivery of anticancer agents. *Molecular Pharmaceutics*, *2*, 194–205.

Kim, D. H., Kim, K. N., Kim, K. M., & Lee, Y. K. (2009). Targeting to carcinoma cells with chitosan- and starch-coated magnetic nanoparticles for magnetic hyperthermia. *Journal of Biomedical Materials Research Part A*, *88A*, 1–11.

Kohler, N., Fryxell, G. E., & Zhang, M. (2004). A bifunctional poly(ethylene glycol) silane immobilized on metallic oxide-based nanoparticles for conjugation with cell targeting agents. *Journal of American Chemical Society*, *126*, 7206–7211.

Leamon, C., & Low, P. (1994). Selective targeting of malignant-cells with cytotoxin-folate conjugates. *Journal of Drug Targeting*, *2*, 101–112.

Liang, X. F., Wang, H. J., Luo, H., Tian, H., Zhang, B. B., Hao, L. J., Teng, J. I., & Chang, J. (2008). Characterization of novel multifunctional cationic polymeric liposomes formed from octadecyl quaternized carboxymethyl chitosan/cholesterol and drug encapsulation. *Langmuir*, *24*, 7147–7153.

Lin, J. J., Chen, J. S., Huang, S. J., Ko, J. H., Wang, Y. M., Chen, T. L., & Wang, L. F. (2009). Folic acid–pluronic F127 magnetic nanoparticle clusters for combined targeting, diagnosis, and therapy applications. *Biomaterials*, *30*, 5114–5124.

Ling, Y., Naggar, A. K., Priebe, W., & Perez-Soler, R. (1996). Cell cycle-dependent cytotoxicity, G2/M phase arrest, and disruption of p34cdc2/cyclin B1 activity induced by doxorubicin in synchronized P388 cells. *Molecular Pharmacology*, *49*, 832–841.

Liu, T. Y., Chen, S. Y., Lin, Y. L., & Liu, D. M. (2006). Synthesis and characterization of amphiphatic carboxymethyl-hexanoyl chitosan hydrogel: Water-retention ability and drug encapsulation. *Langmuir*, *22*, 740–745.

McCarthy, J. R., Kelly, K. A., Sun, E. Y., & Weissleder, R. (2007). Targeted delivery of multifunctional magnetic nanoparticles. *Nanomedicine*, *2*, 153–167.

Mohapatra, S., Mallick, S. K., Maiti, T. K., Ghosh, S. K., & Pramanik, P. (2007). Synthesis of highly stable folic acid conjugated magnetite nanoparticles for targeting cancer cells. *Nanotechnology*, *18*, 385102–385111.

Morris, V. B., & Sharma, C. P. (2010). Folate mediated histidine derivative of quaternised chitosan as a gene delivery vector. *International Journal of Pharmaceutics*, *389*, 176–185.

Narain, R., Gonzales, M., Hoffman, A. S., Stayton, P. S., & Krishnan, K. M. (2007). Synthesis of monodisperse biotinylated p (NIPAAm)-coated iron oxide magnetic nanoparticles and their bioconjugation to streptavidin. *Langmuir*, *23*, 6299–6304.

Okassa, L. N., Marchais, H., Douziech-Eyrolles, L., Herve, K., Cohen-Jonathan, S., Munnier, E., Souce, M., Linassier, C., Dubois, P., & Chourpa, I. (2007). Optimization of iron oxide nanoparticles encapsulation within poly(d,l-lactide-co-glycolide) sub-micron particles. *European Journal of Pharmaceutics and Biopharmaceutics*, *67*, 31–38.

Park, J. H., Maltzahn, G., Zhang, L., Schwartz, M. P., Ruoslahti, E., Bhatia, S. N., & Sailor, M. J. (2008). Magnetic iron oxide nanoworms for tumor targeting and imaging. *Advanced Materials*, *20*, 1630–1635.

Prabaharan, M., & Gong, S. (2008). Novel thiolated carboxymethyl chitosan-g-b-cyclodextrin as mucoadhesive hydrophobic drug delivery carriers. *Carbohydrate Polymers*, *73*, 117–125.

Qian, F., Cui, F., Ding, J., Tang, C., & Yin, C. (2006). Chitosan graft copolymer nanoparticles for oral protein drug delivery: Preparation and characterization. *Biomacromolecules*, *7*, 2722–2727.

Sahu, S. K., Maiti, S., Maiti, T. K., Ghosh, S. K., & Pramanik, P. (2010). Folate decorated succinyl chitosan nanoparticles conjugated with doxorubicin for targeted drug delivery. *Macromolecular Bioscience*, *11*, 285–295.

Sahu, S. K., Maiti, S., Maiti, T. K., Ghosh, S. K., & Pramanik, P. (2011). Hydrophobically modified carboxymethyl chitosan nanoparticles targeted delivery of paclitaxel. *Journal of Drug Targeting*, *19*, 104–113.

Sun, T., Xu, P. X., Liu, Q., Xue, J., & Xie, W. M. (2003). Graft copolymerization of methacrylic acid onto carboxymethyl chitosan. *European Polymer Journal*, *39*, 189–192.

Thierry, B., Kujawa, P., Tkaczyk, C., Winnik, F. M., Bilodeau, L., & Tabrizian, M. (2005). Delivery platform for hydrophobic drugs: Prodrug approach combined with self-assembled multilayers. *Journal of American Chemical Society*, *127*, 1626–1627.

Thierry, B., Winnik, F. M., Merhi, Y., Silver, J., & Tabrizian, M. (2003). Bioactive coatings of endovascular stents based on polyelectrolyte multilayers. *Biomacromolecules*, *4*, 1564–1571.

Wan, S., Huang, J., Guo, M., Zhang, H., Cao, Y., Yan, H., & Liu, K. (2007). Biocompatible superparamagnetic iron oxide nanoparticle dispersions stabilized with poly (ethylene glycol)–oligo (aspartic acid) hybrids. *Journal of Biomedical Materials Research Part A*, *80A*, 946–954.

Wout, Z. G., Pec, E. A., Maggiore, J. A., Williams, R. H., Palicharla, P., & Johnston, T. P. (1992). Poloxamer 407-mediated changes in plasma cholesterol and triglycerides following intraperitoneal injection to rats. *Journal of Parenteral Science and Technology*, *46*, 192–200.

Xie, W. M., Xu, P. X., & Wang, W. (2002). Preparation and antibacterial activity of a water-soluble chitosan derivative. *Carbohydrate Polymers*, *50*, 35–40.

Zhang, J. L., Srivastava, R. S., & Misra, R. D. K. (2007). Core–shell magnetite nanoparticles surface encapsulated with smart stimuli-responsive polymer: Synthesis, characterization, and LCST of viable drug-targeting delivery system. *Langmuir*, *23*, 6342–6351.

Zhang, L., He, R., & Gu, C. (2006). Oleic acid coating on the monodisperse magnetite nanoparticles. *Applied Surface Science*, *253*, 2611–2617.

Zheng, Y., Cai, Z., Song, X., Yu, B., Bi, Y., Chen, Q., Zhao, D., Xu, J., & Ho, S. (2009). Receptor mediated gene delivery by folate conjugated *N*-trimethyl chitosan *in vitro*. *International Journal of Pharmaceutics*, *382*, 262–269.

Zunino, F., & Capranico, G. (1990). DNA topoisomerase II as the primary target of anti-tumor anthracyclines. *Anti-Cancer Drug Design*, *5*, 307–317.